THE JOURNAL OF PHYSICAL CHEMISTRY B

Article

pubs.acs.org/JPCB

Computational Study of the Stability of the Miniprotein Trp-Cage, the GB1 β-Hairpin, and the AK16 Peptide, under Negative Pressure

Harold W. Hatch,[†] Frank H. Stillinger,[‡] and Pablo G. Debenedetti*[,†]

[†]Department of Chemical and Biological Engineering, Princeton University, Princeton, New Jersey 08544, United States

[‡]Department of Chemistry, Princeton University, Princeton, New Jersey 08544, United States

Supporting Information

ABSTRACT: Although hot, cold, and high pressure denaturation are well characterized, the possibility of negative pressure unfolding has received much less attention. Proteins under negative pressure, however, are important in applications such as medical ultrasound, and the survival of biopoloymers in the xylem and adjacent parenchyma cells of vascular plants. In addition, negative pressure unfolding is fundamentally important in obtaining a complete understanding of protein stability and naturally complements previous studies of high pressure denaturation. We use extensive replica-exchange molecular dynamics (REMD) simulations and thermodynamic analysis to obtain folding/unfolding equilibrium phase diagrams for the miniprotein trp-cage (α-structure, 20-residue), the GB1 β-hairpin (β-structure, 16-residue), and the AK16 peptide (α-helix, 16-residue). Although the trp-cage is destabilized by negative pressure, the GB1 β-hairpin and AK16 peptide are stabilized by this condition.

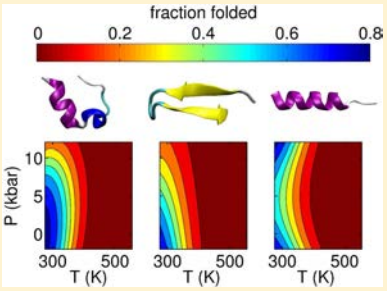

1. INTRODUCTION

In addition to hot, cold, and high pressure denaturation, negative pressure may also denature biomolecules. The attainment of negative pressure requires special experimental techniques.[1,2] A recent study by Larios and Gruebele demonstrates the feasibility of detailed experimental scrutiny of proteins under tension.[3] Medical ultrasound is capable of producing large negative pressures, where high intensity focused ultrasound has been used for noninvasive surgery.[4,5] The effects of negative pressure on proteins in the body due to ultrasound are not well understood at the molecular level. It is important to note that the shape of the stability diagram of proteins in the (P, T) plane has been shown to be similar to that of cells.[6,7] In addition, vascular plants routinely utilize negative pressure to transport water in the xylem. The adjacent parenchyma cells, which are hypothesized to sense and recover from cavitation,[8,9] must survive these tensile stresses. Finally, mechanical forces on proteins in vivo are often investigated with anisotropic tension applied by atomic force microscopes and optical tweezers. There may be fundamental parallels between protein stability under isotropic tension in a solvent (e.g., negative pressure) and anisotropic tension in experimental (e.g., refs 10−12) and simulation (e.g., refs 13−16) studies.

The pressure−temperature stability diagrams of proteins exhibit elliptical shapes, which may be extrapolated to negative pressure with simple two-state thermodynamic models.[17,18] Although a state of negative pressure is metastable with respect to liquid−vapor coexistence, such a condition may be attained and maintained for long times, by not exceeding the maximum tensile strength of the liquid (e.g., the liquid−vapor spinodal).[1,2,19,20] Experimental studies of the pressure stability of proteins typically focus upon high pressure (e.g., ref 7), with applications including food decontamination and refolding of aggregated proteins.[7,21,22] In addition to experimental studies, computer simulations provide insight into the molecular mechanisms of high pressure denaturation.[23,24] Stability diagrams of proteins have also been successfully modeled with analytical theories.[25]

The construction of phase diagrams via molecular simulation is a powerful technique for studying the pressure stability of proteins, with previous studies having considered hot, cold, and high pressure denaturation.[26−31] Although one may extrapolate a thermodynamic model, parametrized with positive pressures, to the negative pressure region, the error in extrapolation is unknown without explicitly conducting simulations at negative pressure. In this work, the focus is upon negative pressure stability. Accordingly, simulations in this work are performed in the negative pressure region. Positive pressure simulations are also reported for comparison with the negative pressure simulations and for quantifying the error in the fit to the thermodynamic model. In addition, the thermodynamic parameters presented in this work that are associated with the pressure dependence of the Gibbs free energy have not been obtained previously for the Amberff03* force field.[32] In contrast to previous work, we obtain three independent measures of pressure stability in the negative pressure regime

Special Issue: James L. Skinner Festschrift

Received: October 28, 2013
Revised: February 20, 2014
Published: February 21, 2014

to avoid extrapolation of the fit to a thermodynamic model parametrized at positive pressure.

An experimental and computational investigation of the stability of a ubiquitin mutant protein at negative pressure was carried out by Larios and Gruebele.[3] The novel experiments involved modification of the NMR cell as a Berthelot tube to probe protein stability at negative pressure. In addition, the change in Gibbs free energy with pressure was obtained by thermodynamic integration of molecular dynamics simulations of an unfolded and a folded protein. The simulation of the unfolded state was represented by a single configuration taken from a thermally denatured state. In contrast, the REMD simulations used in this work with a fast-folding miniprotein overcome kinetic barriers to sample an equilibrium ensemble of folded and unfolded states. This technique, supplemented by a thermodynamic analysis,[30] allows one to obtain the Gibbs free energy surface and its temperature and pressure derivatives in the (P, T) plane.

Here, we investigate the negative pressure stability of the miniprotein trp-cage (α-structure, 20-residue),[33] the GB1 β-hairpin (β-structure, 16-residue),[34] and the AK16 peptide (α-helix, 16 residue)[35] using extensive replica-exchange molecular dynamics (REMD) simulations in explicit water. To our knowledge, this is the first systematic simulation of protein folding in a metastable liquid under isotropic tension. The computational methods are detailed in section 2. In section 3, we show that although the trp-cage is destabilized by negative pressure, the GB1 β-hairpin and AK16 peptide are stabilized at these conditions. Discussion, concluding remarks, and suggestions for further work are included in section 4.

2. COMPUTATIONAL METHODS

2.1. Protein Initial Configurations and Equilibration. A miniprotein, a β-hairpin, and an α-helical peptide were considered in this work to compare the response of different protein structures to negative pressure. The 20-residue trp-cage miniprotein was obtained from the Protein Data Bank (PDB 1L2Y).[33] The 16-residue GB1 β-hairpin was taken from residues 41−56 of the GB1 protein (PDB 1GB1).[34] The α-helical AK16 peptide,[35,36] with the 16-residue one letter amino acid alphabet sequence YGAAKAAAAKAAAAKA, was built with the AmberTools12 program[37] in extended conformation and compacted with a short gas phase simulation. The proteins are modeled with the Amberff03* variant[32] of the Amberff03 force field[38] in explicit TIP3P water.[39] The initial topology files for Gromacs 4 simulation package[40] were generated with the pdb2gmx utility program. Although the termini of the trp-cage and GB1 β-hairpin are not blocked or acetylated, the AK16 peptide was acetylated on the N-terminus and amidated on the C-terminus. The trp-cage was solvated in 1201 water molecules, 7 sodium ions, and 8 chloride ions. The number of ions was chosen to match the concentration used in previous simulations.[41] To demonstrate system size independence (Supporting Information), a second trp-cage protein simulation was solvated in 2402 water molecules, 14 sodium ions, and 15 chloride ions. GB1 β-hairpin was solvated in 984 water molecules, 6 sodium ions, and 3 chloride ions. A second GB1 β-hairpin simulation was solvated in 1968 water molecules, 9 sodium ions, and 6 chloride ions. AK16 peptide was solvated in 1213 water molecules and 3 chloride ions. All simulations were conducted with truncated octahedron periodic boundary conditions,[42] such that the volume of the system is a factor of $4/9(\sqrt{3})$ smaller than a cubic box with the same maximum length.

The initial configurations were equilibrated as detailed below to obtain a few different isochoric configurations to span the pressure range of −1.5 to +20 kbar and temperature range of 275−580 K in constant-volume REMD simulations. The initial structures were briefly energy minimized with 100 steps to move overlapping atoms. The solvent was then equilibrated at 300 K using the Berendsen thermostat[43] for 1 ps while position-restraining the protein. The water molecules were treated as rigid with the SETTLE algorithm[44] with a 2 fs time step. Short-range interactions were cut off at 0.9 nm. The long-range electrostatics were calculated by the Particle Mesh Ewald technique (PME[45]) with a 0.12 nm grid spacing. The entire system was then equilibrated for 10 ps, and all protein bonds were constrained with the LINCS algorithm.[46] The final configurations to be used in constant-volume REMD simulations were obtained via 1 ns simulations at a few selected pressures ranging from −1 to 10 kbar with the Berendsen barostat[43] at 300 K, resulting in the following densities: 0.96, 0.99, and 1.15 g/mL for the trp-cage miniprotein with 1201 water molecules, 0.98 g/mL for the trp-cage miniprotein with 2402 water molecules (equivalent pressure as 0.99 g/mL for 1201 water molecules), 0.96, 1.01, and 1.15 g/mL for GB1 β-hairpin with 984 water molecules, 0.99 g/mL for GB1 β-hairpin with 1968 water molecules (equivalent pressure as 1.01 g/mL for 984 water molecules), and 0.93, 1.16, and 1.26 g/mL for the AK16 peptide. The Berendsen thermostat and barostat were used only in equilibration and not in production simulations. Density is defined as the total mass of the system divided by the total volume. Note that in these simulations, the volume of the protein is non-negligible compared to the volume of the water, and therefore the pressure is a more experimentally comparable variable (e.g., Figures 4−6) than density.

2.2. Replica-Exchange Molecular Dynamics (REMD). Replica-exchange molecular dynamics (REMD) simulations enhance sampling of the folding/unfolding transitions in the miniproteins and peptides.[47−49] The temperature was controlled with stochastic dynamics[50,51] and density was held fixed. Temperature ranges for nearly constant acceptance ratios were obtained from a few iterations of short, 100 ps REMD simulations with a fast, 0.02 ps exchange rate. For the trp-cage, 2 isochores of 0.96 and 0.99 g/mL were simulated for 1.25 μs per replica and the isochore 1.15 g/mL was simulated for 1.1 μs per replica, each with 32 replicas in the temperature range 276−579 K with exchange acceptance ratios of 20−23%. To demonstrate convergence of the equilibrium folded population independent of initial configuration (Supporting Information), another trp-cage simulation was initialized from an ensemble of unfolded configurations of the 579 K replica, 0.96 g/mL, and simulated for 0.65 μs. For the trp-cage simulation with 2402 water molecules, 0.99 g/mL, 32 replicas were simulated for 0.5 μs per replica in the temperature range 285−533 K with exchange acceptance ratios of 12−15%. For GB1 β-hairpin, 4 isochores of 0.96, 1.01, 1.15, and 1.27 g/mL with 24 replicas each were simulated for 1 μs per replica in the temperature range 282.5−550 K with exchange acceptance ratios of 15−19%. For the GB1 β-hairpin simulation with 2402 water molecules, 1.01 g/mL, 30 replicas were simulated for 0.5 μs per replica in the temperature range 285−545 K with exchange acceptance ratios of 12−15%. For AK16 peptide, 2 isochores of 0.93 and 1.26 g/mL were simulated for 1 μs with 24 replicas in

dx.doi.org/10.1021/jp410651u | J. Phys. Chem. B 2014, 118, 7761−7769

the temperature range 285−542 K with exchange acceptance ratios of 12−15%, and the isochore 1.16 g/mL was simulated for 0.5 μs, with 24 replicas in the temperature range 285−492 K with exchange acceptance ratios of 20−25%. In addition, the change in volume upon unfolding was obtained by additional 100 ns REMD simulations in the constant-pressure (NPT) ensemble at the same series of temperatures and pressures as the NVT REMD simulations, by using the Parrinello−Rahman barostat[52] and starting from the final NVT configurations. An exchange rate of 1 ps was used for production REMD simulations, except for the 10 ps exchange rate in the first 250 ns of the trp-cage simulations with 1201 water molecules at 0.99 and 0.96 g/mL. The REMD simulations utilized the same time step, constraint algorithms, interaction cut off and electrostatics as described in section 2.1. Configurations were stored for analysis every 1 ps for non-hydrogen protein atoms, and every 100 ps for the entire configuration to save disk space. Temperature, potential energy, pressure and volume were also stored every 1 ps.

2.3. Protein Structural Analysis. The protein structure was characterized with order parameters d_{RMS}, Q_{bb}, rmsd, and STRIDE[53] to distinguish folded and unfolded states. The distance-based root-mean-squared deviation, d_{RMS}, is defined as $d_{\mathrm{RMS}} = [N_{\mathrm{bb}}{}^{-1}\sum_{i,j}(r_{ij} - r_{ij,0})^2]^{1/2}$, where i and j are integer indices for sequential numbering along the backbone carbon, nitrogen or oxygen atoms, and the sum is over all pairs of the N_{bb} backbone atom native contacts. Native contacts are defined as all pairwise backbone atom separation distances, $r_{ij,0}$, in a reference structure (first entry of PDB) where $r_{ij,0} < 0.45$ nm and atom pairs i and j must belong to different residues that are separated by two or more residues along the backbone. The fraction of backbone native contacts, Q_{bb}, is defined as $Q_{\mathrm{bb}} = N_{\mathrm{bb}}{}^{-1}\sum_{i,j}\{1 + \exp[\beta(r_{ij} - \lambda r_{ij,0})]\}^{-1}$, where $\beta = 0.5$ nm^{-1} and $\lambda = 1.2$, as described previously.[41] The root-mean-squared deviation, rmsd, from a least-squares fitted reference structure (first entry of PDB) is defined as rmsd $= M^{-1}\sum_1 m_i|\vec{r}_i - \vec{r}_{i,0}|^2]^{1/2}$, where the sum is over all protein backbone carbon, nitrogen or oxygen atoms, $M = \sum_i^{\mathrm{bb}} m_i$, m_i is the mass, $\vec{r}_i$ is the instantaneous position, and $\vec{r}_{i,0}$ is the position of the least-squares fitted reference structure. Free energy profiles and surfaces of order parameters were computed via $-RT\ln(p)$, where R is the gas constant, T is the temperature, and p represents a probability assigned for a chosen order parameter, obtained from histograms. The two-dimensional histograms were fitted to a surface and smoothed with Gaussian functions.

For the trp-cage, folded states are defined as rmsd < 0.22 nm[30] (Figure 1). For GB1 β-hairpin, folded states are defined as $d_{\mathrm{RMS}} < 0.15$ nm[41] (Figure 2). As opposed to the trp-cage and GB1 β-hairpin, the ensemble of helical (folded) states for the AK16 peptide is structurally diverse. The folded state was defined as structures with 50% or more residues in helical conformations assigned using the STRIDE algorithm[53] implemented in the VMD program.[54] A closely related definition of fraction folded as a fraction of helical residues, as employed previously,[36] yields a similar folding curve (Supporting Information).

2.4. REMD Convergence. An important quantity that is computed by the REMD simulations is the fraction of time that a replica, at a given temperature, is in the folded state. This fraction of time folded is equivalent, in the thermodynamic limit, to an ensemble average fraction of folded proteins, as measured in experiments at high protein dilution. Folding/unfolding equilibrium convergence is evidenced from the fraction of folded proteins in all replicas as a function of time, as shown in the Supporting Information. For the trp-cage, the correlation time of the fraction of folded proteins in all replicas is 50 ns, estimated as twice the maximum value of the integral of the correlation function (Supporting Information).[42,55] The correlation times for GB1 β-hairpin and AK16 peptide are 50 and 10 ns, respectively. Error bars in the thermodynamic fits (e.g., Figure 3) are standard deviations of the mean obtained from block averages of twice the correlation time.[55,56] The first 250 ns of REMD simulation are discarded as equilibration, except for the cases described below. The trp-cage simulations with the initial 250 ns of the slower 10 ps exchange rate were given an additional 250 ns (500 ns total) equilibration. In addition, a longer equilibration time of 400 ns was required for the initially unfolded trp-cage simulation because the unfolded initial condition is further from the equilibrium fraction folded in the slowest, low temperature replicas, as opposed to the folded initial condition. Convergence of the equilibrium folded population independent of the folded or unfolded initial configuration for the trp-cage miniprotein at 0.96 g/mL is shown in the Supporting Information. In addition, see the Supporting Information for system size independence of the fraction of folded trp-cage and GB1 β-hairpin as a function of temperature.

2.5. Fit to Thermodynamic Model. A two-state thermodynamic model of the change in the Gibbs free energy upon unfolding[17,18] is fitted to the REMD simulation data for a range of temperatures and pressures.[30,31] The change in the Gibbs free energy is given by

$$\Delta G = G_{\mathrm{u}} - G_{\mathrm{f}} = -RT\ln((1-x)/x) \tag{1}$$

where the subscript u refers to the unfolded state, the subscript f refers to the folded state, x is the ensemble average of the fraction of the proteins in the native state, T is the temperature, and R is the ideal gas constant. Note that in the infinite dilution simulations in this work, the fraction of time folded is equivalent to x. To obtain the free energy surface, one integrates $d(\Delta G) = -\Delta S\, dT + \Delta V\, dP$, where S is the entropy, $\Delta S = S_{\mathrm{u}} - S_{\mathrm{f}}$, V is the volume, $\Delta V = V_{\mathrm{u}} - V_{\mathrm{f}}$, and P is the pressure. Integration is performed from a state T_0, P_0 to T, P while assuming that the second order derivatives of ΔG are constant and given by

$$\Delta\alpha = \left.\frac{\partial}{\partial T}\right|_P \left.\frac{\partial \Delta G}{\partial P}\right|_T = \left.\frac{\partial \Delta V}{\partial T}\right|_P \tag{2}$$

$$\Delta\beta = \left.\frac{\partial^2 \Delta G}{\partial^2 P}\right|_T = \left.\frac{\partial \Delta V}{\partial P}\right|_T \tag{3}$$

$$\Delta C_P = -T\left.\frac{\partial^2 \Delta G}{\partial^2 T}\right|_P = T\left.\frac{\partial \Delta S}{\partial T}\right|_P \tag{4}$$

Note that the symbols $\Delta\alpha$ and $\Delta\beta$ used here, as defined previously,[17] are related to, but not the same as, the thermal expansion coefficient and compressibility. To integrate $d(\Delta G)$, one first integrates $d(\Delta S)$ and $d(\Delta V)$ to obtain the following expressions,

$$\Delta S = \Delta C_P \ln(T/T_0) - \Delta\alpha(P - P_0) + \Delta S_0 \tag{5}$$

$$\Delta V = \Delta\alpha(T - T_0) + \Delta\beta(P - P_0) + \Delta V_0 \tag{6}$$

dx.doi.org/10.1021/jp410651u | J. Phys. Chem. B 2014, 118, 7761−7769

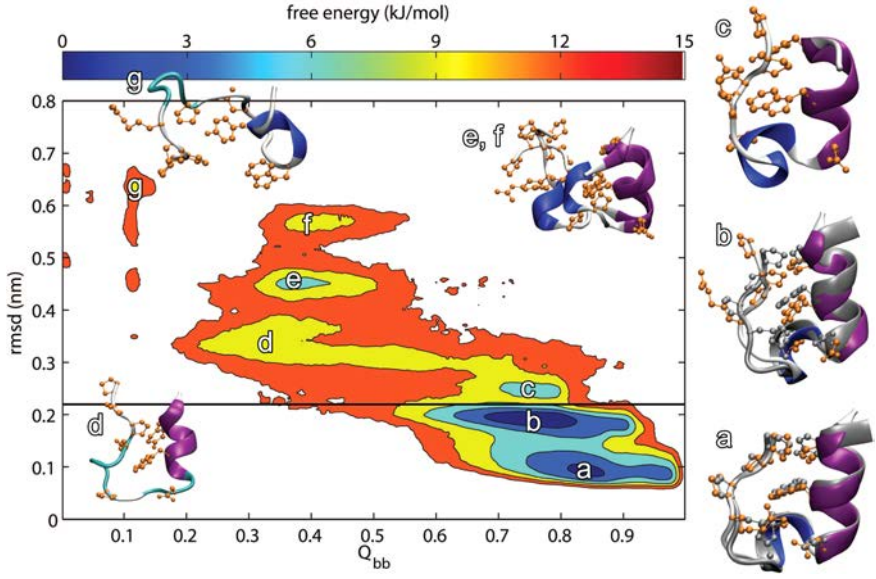

Figure 1. Free energy surface of the trp-cage at 299 K and 0.99 g/mL as a function of the fraction of native backbone contacts, Q_{bb}, and the backbone rmsd. Folded states are defined as rmsd <0.22 nm, shown by the black line in the free energy surface contour plot. Protein structures are representative of the local minima indicated in the free energy surface contour plot and are shown with the following STRIDE[53] secondary structure assignments: α-helix in magenta, 3_{10}-helix in dark blue, coil in white, and turn in teal. Proline, tryptophan, tyrosine, arginine, and aspartic acid heavy side chain atoms are shown in gold. Structures "a" and "b" include the overlapping 1L2Y PDB[33] shown in silver.

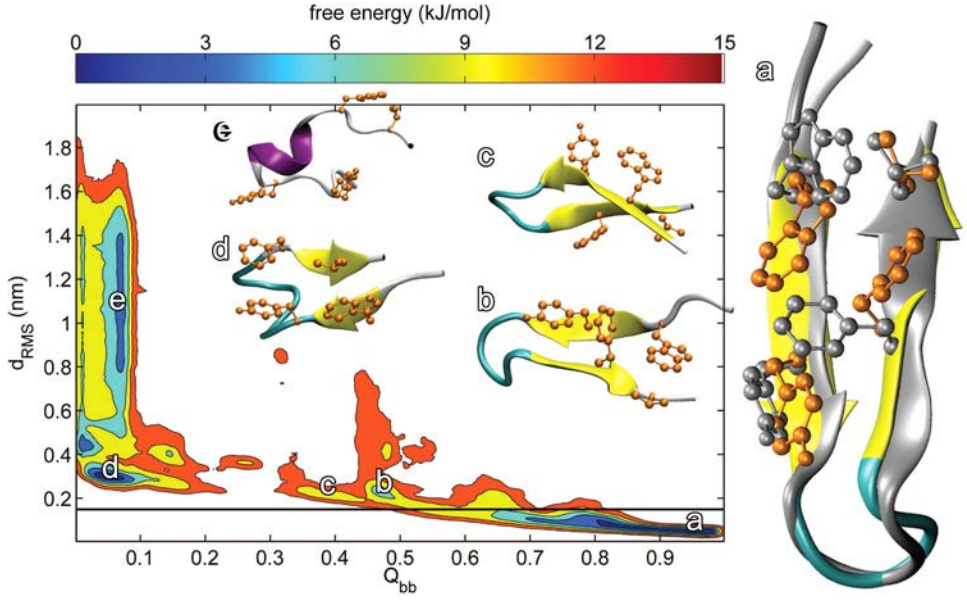

Figure 2. Free energy surface of GB1 β-hairpin at 297 K and 1.01 g/mL, similar to Figure 1, except that folded states are defined as d_{RMS} < 0.15 nm. Tryptophan, tyrosine, phenylalanine, and valine heavy side chain atoms are shown in gold. Structure "a" includes the overlapping 1GB1 PDB[34] shown in silver.

Finally, inserting the expressions for ΔS and ΔV to integrate $d(\Delta G)$,

$$\Delta G = \Delta G_0 - \Delta S_0(T - T_0) + \Delta V_0(P - P_0) + \frac{\Delta\beta}{2}(P - P_0)^2 + \Delta\alpha(T - T_0)(P - P_0) - \Delta C_P[T \ln(T/T_0) - (T - T_0)] \quad (7)$$

Note that the contours of constant ΔG are elliptical near T_0 when $(\Delta\alpha)^2 > \Delta C_P\Delta\beta/T_0$.[17] This free energy surface may be fitted to two different data sets from REMD simulations. First, the fraction folded, x, at a given T, P gives ΔG via eq 1, which is then used to fit to eq 7. The second data set from simulations is ΔE, which may be fitted to the equation $\Delta E = \Delta G + T\Delta S - P\Delta V$ obtained via eqs 5−7. The thermodynamic fits were performed in Mathematica 8 by minimization of the squared deviation of the fit to ΔG, ΔE, and x, weighted by the standard deviation. Note that $\Delta G \sim \Delta A$, where A is the Helmholtz free energy, because $P\Delta V$ is small[30] (Figure 3 and Supporting Information). All thermodynamic quantities are on a per mole of protein basis.

2.6. Estimate of Spinodal of Bulk Water. A simple method was used to estimate the spinodal of bulk water, which serves merely as a reference in the stability diagrams. The

dx.doi.org/10.1021/jp410651u | J. Phys. Chem. B 2014, 118, 7761−7769

spinodal of bulk water was estimated for a given temperature by gradually lowering the pressure in an *NPT* molecular dynamics simulation until the system became unstable due to rapid expansion. The initial system contained 1728 water molecules in cubic periodic boundary conditions. The Berendsen thermostat and barostat[43] were used with time constants of 0.1 and 0.5 ps, respectively. Each constant pressure simulation was preformed for 40 ps with a 2 fs time step, and the pressure was then decreased by 10 bar. The spinodal pressure was obtained as the lowest pressure reached before rapid expansion.

3. RESULTS

Replica-exchange molecular dynamics (REMD) simulations are used for the folding of the trp-cage, GB1 β-hairpin, and AK16 peptide in explicit water to compute their pressure−temperature stability diagrams. The two-state thermodynamic description depends upon a physically reasonable order parameter to partition the protein structures. First, we show that rmsd <0.22 nm and d_{RMS} < 0.15 nm (see definition in section 2.3) describe well the folded states of the trp-cage and GB1 β-hairpin, respectively.[30,41] Then we fit the simulation data in the $P-T$ plane to a two-state thermodynamic model (eq 7) to obtain the stability diagrams of the trp-cage, GB1 β-hairpin, and AK16 peptide.

Representative protein structures from the folding/unfolding equilibrium, along with free energy surfaces as a function of the fraction of backbone native contacts, Q_{bb}, and backbone rmsd for the trp-cage, and backbone d_{RMS} for GB1 β-hairpin, are shown in Figures 1 and 2, respectively. For the trp-cage, folded states are defined as rmsd <0.22 nm and closely resemble the NMR structure (PDB ID 1L2Y).[33] The folded trp-cage structure is stabilized by a combination of the "caged" tryptophan nonpolar residue, the arginine−aspartic acid salt bridge, favorable helical regions, and the rigidity of proline.[33] Structures "a" and "b" are virtually identical, as reported previously,[31,41] and are due to minor differences in the backbone dihedral angles of GLY[15] and absence of the ASP[9]-ARG[16] salt bridge in structure "b". Structure "c" is considered unfolded, however, because LEU[2] is not in a helical conformation. Note that rmsd distinguishes structure "c" from "a" and "b", whereas Q_{bb} does not. The contracted, one-dimensional free energy profile as a function of rmsd can be found in the Supporting Information.

For the GB1 β-hairpin, folded states are defined as d_{RMS} < 0.15 nm and closely resemble the NMR structure (PDB ID 1GB1).[34] In contrast to the trp-cage, the folded GB1 β-hairpin structure is composed of β-strands. Comparing the most predominant conformation from simulations (e.g., structure "a" of Figure 2) to the 1GB1 PDB,[34] we note that the nonpolar side chains are slightly distorted due to the absence, in our calculations, of favorable contacts with residues in the full 1GB1 protein (see also section 2.1). The free energy surfaces do not necessarily provide a physical transition path between states. For example, despite the intermediate Q_{bb} value, GB1 β-hairpin structure "c" of Figure 2 is a misfold and must unravel before correctly folding because one of the β-strands in "c" is flipped with respect to "a".[41]

The fit of the simulation data to a two-state thermodynamic model (eq 7) and the resulting pressure−temperature stability diagram are illustrated for GB1 β-hairpin in Figures 3 and 4, respectively. The GB1 β-hairpin is stabilized by the application of negative pressure, as evidenced by the slope of the contours of constant fraction folded. The negative pressure stabilization

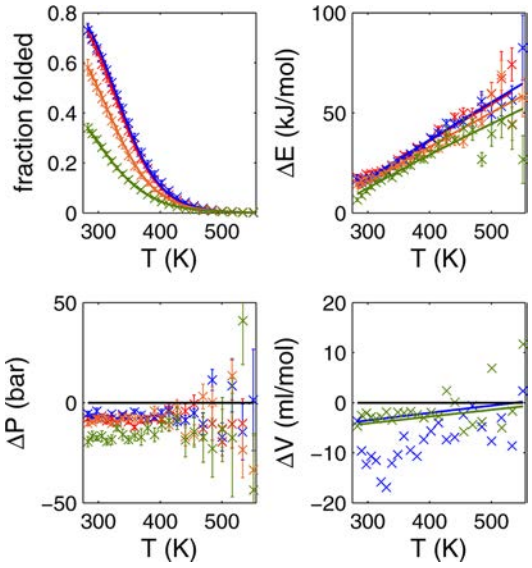

Figure 3. Fit of GB1 β-hairpin simulation data (points with error bars) to two-state thermodynamic model (lines, section 2.5). Colors denote the following isochores: 0.96 g/mL (blue), 1.01 g/mL (red), 1.15 g/mL (orange), and 1.27 g/mL (green). Top left: Fraction of folded GB1 β-hairpins. Top right: Change in potential energy upon unfolding. Bottom left: Change in pressure. Bottom right: Change in volume. As T increases, the error bars become larger when $x \to 0$. Although the precise magnitude of ΔP and ΔV are statistically difficult to compute due to incompressibility of the liquid, their sign is more easily determined. The black lines, $\Delta P = 0$ and $\Delta V = 0$, serve as a guide to the eye.

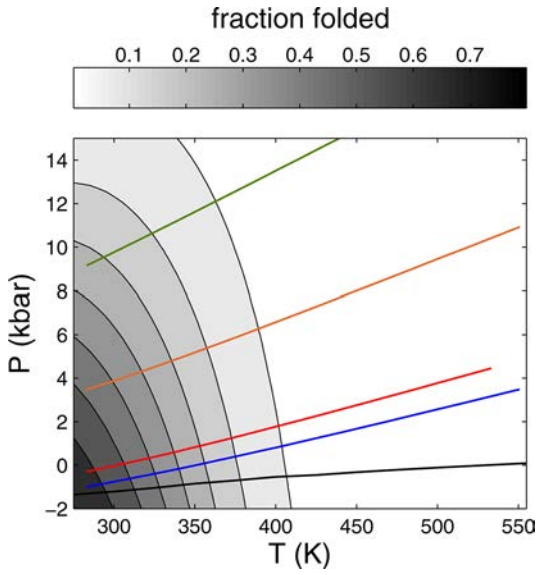

Figure 4. Stability diagram of GB1 β-hairpin by fit of simulation data (colored lines) to two-state thermodynamic model, with contours of fraction folded in intervals of 0.1. Colored lines are for densities described in Figure 3. The black line is a numerical estimate of the spinodal of the bulk water system (section 2.6).

of GB1 β-hairpin is confirmed by three sets of data. First, the fraction folded increases from the second lowest to the lowest density ischore. A second measure of the pressure stability of GB1 β-hairpin is ΔP, the change in pressure upon unfolding in the *NVT* simulations (section 2.2). If $\Delta P = -\partial \Delta A/\partial V|_T < 0$, where Δ denotes the difference in a given quantity between

dx.doi.org/10.1021/jp410651u | J. Phys. Chem. B 2014, 118, 7761−7769

unfolded and folded states, the free energy difference between the unfolded and folded states increases if the volume increases. The converse is true if $\Delta P > 0$. If $\Delta P < 0$, this implies that upon increasing the volume or, equivalently, decreasing the pressure, the folded state is stabilized ($\Delta\Delta A > 0$) relative to the unfolded state. Finally, $\Delta V = \partial\Delta G/\partial P|_T < 0$ from NPT simulations (section 2.2) also confirms that GB1 β-hairpin is stabilized by the application of negative pressure. In all cases examined, ΔV and ΔP have the same sign at the same state conditions (Supporting Information). ΔV is more physically intuitive, however, because the magnitude of ΔP depends on technical details of the simulation, such as the number of water molecules solvating the protein (section 2.5).

Stability diagrams of the trp-cage and AK16 peptide are shown in Figures 5 and 6, respectively. These stability diagrams

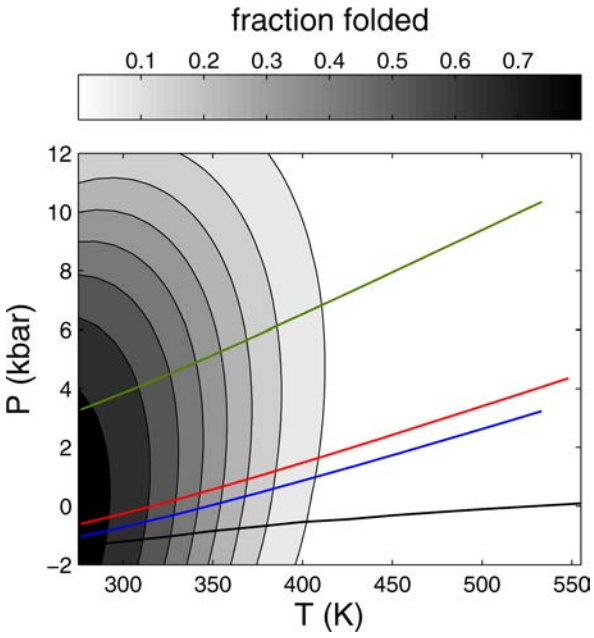

Figure 5. Stability diagram of the trp-cage, similar to Figure 4, except that colors denote the following isochores: 0.96 g/mL (blue), 0.99 g/mL (red), and 1.15 g/mL (green).

were produced by the same fitting procedure as illustrated by Figure 3 (Supporting Information). Although the trp-cage is destabilized by negative pressure, the AK16 peptide is stabilized under the same conditions. The converse is true at high pressure. Figure 7 shows opposing pressure stability of the two folded structures "a" and "b" of the trp-cage (Figure 1). The one-dimensional free energy profile of the trp-cage as a function of rmsd was computed via $-RT\ \ln(p)$, where R is the gas constant, T is the temperature, and p represents a probability assigned for a chosen order parameter, obtained from histograms. Structure "a" is stabilized at higher pressure, whereas structure "b" is stabilized at lower pressure.

The thermodynamic parameters, defined in section 2.5, are summarized in Table 1 and compared with available experimental values. The estimated error in the last digit of the thermodynamic parameters is in the parentheses of Table 1 (Supporting Information). The second derivatives of the Gibbs free energy with at least one derivative in pressure, $\Delta\alpha$ and $\Delta\beta$, are subject to largest uncertainty of all the reported thermodynamic variables. For example, exclusion of the highest density isochore simulation in the GB1 β-hairpin fit yields re-

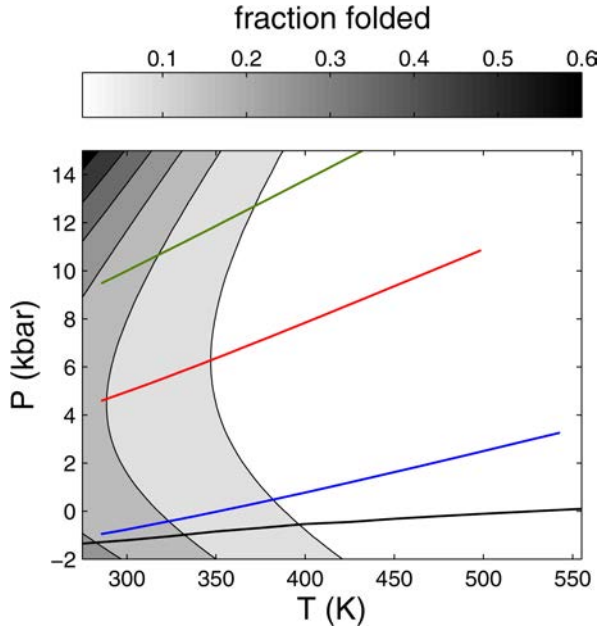

Figure 6. Stability diagram of AK16 peptide, similar to Figure 4, except that colors denote the following isochores: 0.93 g/mL (blue), 1.16 g/mL (red), and 1.26 g/mL (green).

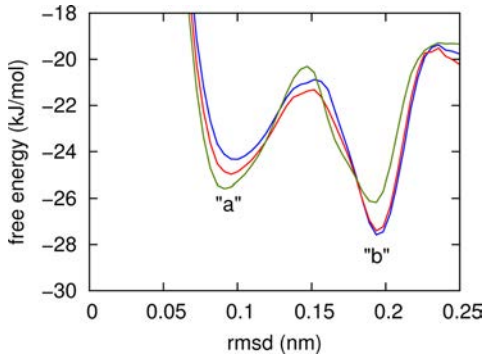

Figure 7. Free energy profile of the folded state structures "a" and "b" of the trp-cage (Figure 1) at 299 K as a function of the backbone rmsd for the following isochores: 0.96 g/mL (blue), 0.99 g/mL (red), and 1.15 g/mL (green).

entrant behavior ($\Delta\beta > 0$) with an island of stability at large pressure, shown in Figure 8. Note that a possible island of stability was also reported by extrapolation to large negative pressure by Larios and Gruebele.[3] The extrapolations rely upon accurately quantifying the second derivatives of the change in the Gibbs free energy upon unfolding, which are numerically small and subject to large statistical error. As reported previously,[31] the entropy change from the simulations is smaller than what is found in experiment.

Figure 9 illustrates how the behavior of the trp-cage and GB1 β-hairpin under negative pressure is related to the position of the center of the elliptical stability diagram relative to the spinodal. For example, the center of the trp-cage ellipse is high enough with respect to the spinodal to observe low pressure unfolding, whereas the center of the GB1 β-hairpin ellipse is much lower than the spinodal such that only high pressure unfolding may be observed.

dx.doi.org/10.1021/jp410651u | J. Phys. Chem. B 2014, 118, 7761−7769

Table 1. Thermodynamic Parameters for the Two-State Model

	trp		GB1-β		AK16	
	sim[a]	exp[b57]	sim	exp[58]	sim	exp[35]
T_0, P_0 (K, bar)	298, 1	298, 1	297, 1	297, 1	298, 1	298, 1
ΔG_0 (kJ/mol)	3.1 (6)	3.2 (2)	1.5 (3)	0	−2.9 (2)	
ΔS_0 (J/mol/K)	49 (2)	160 (6)	49 (1)	160	34 (1)	
ΔV_0 (ml/mol)	0.6 (2)		−3.6 (6)		−3.4 (6)	10.5 (3)
$\Delta\alpha$ [(mL/mol)/K]	0.03 (1)		0.016 (2)		−0.023 (6)	
$\Delta\beta$ [(mL/mol)/bar]	$-1.0(4) \times 10^{-4}$		$-6(6) \times 10^{-5}$		$7(2) \times 10^{-4}$	
ΔC_P [(kJ/mol)/K]	0.31 (1)	0.3 (1)	0.203 (7)		0.086 (3)	
T_f^c (K)	342 (5)	318 (1)	323 (3)	297	213 (2)	

[a]Sim is the abbreviation for simulations from this work. [b]Exp is the abbreviation for experiments from other studies. [c]T_f is the temperature where $\Delta G(T_f P_0) = 0$.

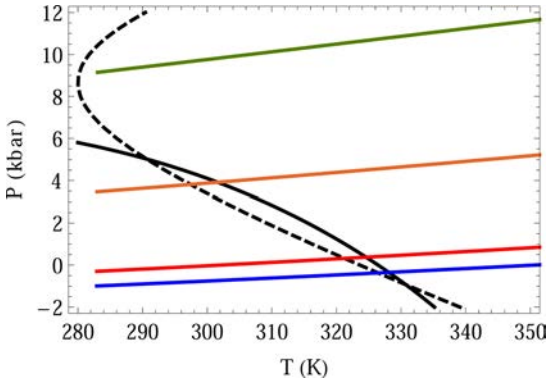

Figure 8. Illustration of re-entrant phase behavior as an artifact of extrapolation for the GB1 β-hairpin. Colored lines denote simulations at the following isochores: 0.96 g/mL (red), 1.01 g/mL (blue), 1.15 g/mL (yellow), and 1.27 g/mL (green). The solid black line is the locus of 0.5 fraction folded, obtained by fit to all isochores, and the dashed black line was obtained by fit to only the three lowest density isochores.

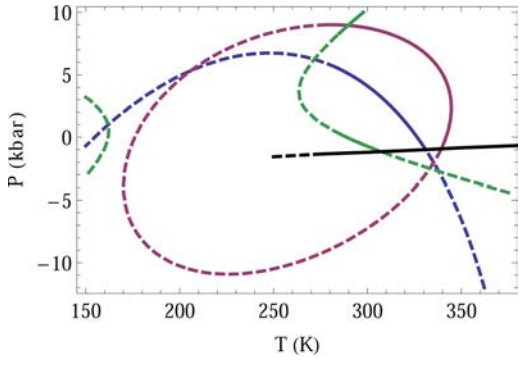

Figure 9. Colored lines are the loci of 0.5 fraction folded for the trp-cage (magenta) 0.5 fraction folded for GB1 β-hairpin (blue) and 0.25 fraction folded for AK16 peptide (green). Dashed lines indicate extrapolation of the thermodynamic model, and unbroken lines are in the vicinity of simulation data. The black line is a numerical estimate of the spinodal of the bulk solution.

4. DISCUSSION AND CONCLUDING REMARKS

To our knowledge, this is the first systematic simulation study of protein folding in a metastable liquid under isotropic tension (negative pressure). We found that the effect of negative pressure on stability depends on the structure of the protein, and each of the three peptides considered exhibts a different stability diagram in the $P-T$ plane. Although the trp-cage is destabilized by application of negative pressure, the GB1 β-hairpin and AK16 peptide are stabilized by the same condition.

Comparison of the simulation results to experiment are important in validation of the protein model. Though the temperature derivatives of the change in Gibbs free energy, ΔS_0 and ΔC_P, may be favorably compared with experiment (Table 1), experimental results for both high and low pressure dependence of the change in Gibbs free energy for the trp-cage and GB1 β-hairpin are lacking. Some pressure stability data for larger proteins are available. However, simulations of protein folding for explicit water, all-atom models are only computationally feasible for fast-folding, smaller miniproteins and peptides, such as those considered in this work (see, however, ref 59). Experimental studies of the pressure stability of miniproteins and peptides would aid in the validation and improvement of all-atom explicit water−protein models. For AK16 peptide, simulations with both Amber03* and CHARMM22[36] find ΔV_0 to have the opposite sign as in experiment[35] (Table 1); however, simulations at high pressure give the correct sign for ΔV. Interestingly, one other case where high pressure simulation results agreed with ambient pressure experiments better than ambient pressure simulations is when structure "a", most closely resembling the NMR structure of the trp-cage,[33] was more favored at higher pressures (Figures 1 and 7). One possible explanation is that the equation of state of TIP3P water utilized in both the Amber03* and CHARMM22 force fields underestimates the density of water relative to experiment at $T > 280$ K and $P = 1$ bar.[60] Protein simulations may benefit from the use of improved water models,[61,62] such as Amber ff03w optimized for simulations with TIP4P/2005.[63]

An intriguing extension of this work is to investigate the effect of cosolutes on the pressure stability of proteins. Experimentally, it was found that crowding increased the pressure stability of staphylococcal nuclease.[64] It is not understood how the shape of the protein stability diagram (e.g., Figure 9) changes upon the addition of denaturants, stabilizers or crowding agents (e.g., does the elliptical diagram shrink or expand with denaturants and stabilizers, respectively, or does the center of the ellipse shift?). The computation of protein stability diagrams with all-atom protein models[30] is clearly a powerful technique that may be applied to understand many of these questions.

■ ASSOCIATED CONTENT

Supporting Information

Additional data including simulation convergence, protein structural order parameters, complete thermodynamic fits,

dx.doi.org/10.1021/jp410651u | J. Phys. Chem. B 2014, 118, 7761−7769

and error analysis are provided. This material is available free of charge via the Internet at http://pubs.acs.org/.

AUTHOR INFORMATION

Corresponding Author

*P. G. Debenedetti: e-mail, pdebene@princeton.edu.

Notes

The authors declare no competing financial interest.

ACKNOWLEDGMENTS

The financial support of the National Science Foundation (Grant No. CHE-1213343 to P.G.D. and Graduate Fellowship to H.W.H.) is gratefully acknowledged. We are grateful to Angel E. Garcia for providing thermodynamic trp-cage simulation data and analysis code for comparison, and to Jeetain Mittal for helpful discussions. The authors are pleased to acknowledge that the work reported on in this paper was substantially performed at the TIGRESS high performance computer center at Princeton University, which is jointly supported by the Princeton Institute for Computational Science and Engineering and the Princeton University Office of Information Technology.

REFERENCES

(1) Zheng, Q.; Durben, D. J.; Wolf, G. H.; Angell, C. A. Liquids at Large Negative Pressures: Water at the Homogeneous Nucleation Limit. *Science* **1991**, *254*, 829−832.

(2) Imre, A. R.; Maris, H. J.; Williams, P. R. *Liquids Under Negative Pressure*; Springer: Berlin, 2002.

(3) Larios, E.; Gruebele, M. Protein Stability at Negative Pressure. *Methods* **2010**, *52*, 51−56.

(4) Sanghvi, N. T.; Foster, R. S.; Bihrle, R.; Casey, R.; Uchida, T.; Phillips, M. H.; Syrus, J.; Zaitsev, A. V.; Marich, K. W.; Fry, F. J. Noninvasive Surgery of Prostate Tissue by High Intensity Focused Ultrasound: An Updated Report. *European Journal of Ultrasound* **1999**, *9*, 19−29.

(5) Wu, F.; Wang, Z.-B.; Cao, Y.-D.; Chen, W.-Z.; Bai, J.; Zou, J.-Z.; Zhu, H. A Randomised Clinical Trial of High-Intensity Focused Ultrasound Ablation for the Treatment of Patients with Localised Breast Cancer. *Br. J. Cancer* **2003**, *89*, 2227−2233.

(6) Butz, P.; Ludwig, H. Pressure Inactivation of Microorganisms at Moderate Temperatures. *Physica B+C* **1986**, *140*, 875−877.

(7) Markley, J. L.; Northrop, D. B.; Royer, C. A. *High Pressure Effects in Biophysics and Enzymology*; Oxford University Press: Oxford, U.K., 1996.

(8) Salleo, S.; Lo Gullo, M. A.; Trifil, P.; Nardini, A. New Evidence for a Role of Vessel-Associated Cells and Phloem in the Rapid Xylem Refilling of Cavitated Stems of Laurus Nobilis L. *Plant, Cell & Environment* **2004**, *27*, 1065−1076.

(9) Secchi, F.; Gilbert, M. E.; Zwieniecki, M. A. Transcriptome Response to Embolism Formation in Stems of Populus Trichocarpa Provides Insight into Signaling and the Biology of Refilling. *Plant Physiol.* **2011**, *157*, 1419−1429.

(10) Fernandez, J. M.; Li, H. Force-Clamp Spectroscopy Monitors the Folding Trajectory of a Single Protein. *Science* **2004**, *303*, 1674−1678.

(11) Berkovich, R.; Hermans, R. I.; Popa, I.; Stirnemann, G.; Garcia-Manyes, S.; Berne, B. J.; Fernandez, J. M. Rate Limit of Protein Elastic Response Is Tether De- pendent. *Proc. Natl. Acad. Sci.* **2012**, 14416−14421.

(12) Popa, I.; Kosuri, P.; Alegre-Cebollada, J.; Garcia-Manyes, S.; Fernandez, J. M. Force Dependency of Biochemical Reactions Measured by Single-Molecule Force-Clamp Spec- troscopy. *Nat. Protoc.* **2013**, *8*, 1261−1276.

(13) Best, R. B.; Hummer, G. Protein Folding Kinetics Under Force from Molecular Simu- lation. *J. Am. Chem. Soc.* **2008**, *130*, 3706−3707.

(14) Best, R. B.; Paci, E.; Hummer, G.; Dudko, O. K. Pulling Direction as a Reaction Coordinate for the Mechanical Unfolding of Single Molecules. *J. Phys. Chem. B* **2008**, *112*, 5968−5976.

(15) Li, J.; Fernandez, J. M.; Berne, B. J. Waters Role in the Force-Induced Unfolding of Ubiquitin. *Proc. Natl. Acad. Sci.* **2010**, *107*, 19284−19289.

(16) Stirnemann, G.; Giganti, D.; Fernandez, J. M.; Berne, B. J. Elasticity, Structure, and Relaxation of Extended Proteins Under Force. *Proc. Natl. Acad. Sci.* **2013**, 3847−3852.

(17) Hawley, S. A. Reversible Pressure-Temperature Denaturation of Chymotrypsinogen. *Biochemistry* **1971**, *10*, 2436−2442.

(18) Smeller, L. Pressure-Temperature Phase Diagrams of Biomolecules. *Biochim. Biophys. Acta* **2002**, *1595*, 11−29.

(19) Caupin, F.; Arvengas, A.; Davitt, K.; Azouzi, M. E. M.; Shmulovich, K. I.; Ramboz, C.; Sessoms, D. A.; Stroock, A. D. Exploring Water and Other Liquids at Negative Pressure. *J. Phys.: Condens. Matter* **2012**, *24*, 284110−284110-7.

(20) Azouzi, M. E. M.; Ramboz, C.; Lenain, J.-F.; Caupin, F. A Coherent Picture of Water at Extreme Negative Pressure. *Nat. Phys.* **2012**, *9*, 38−41.

(21) John, R. J. S.; Carpenter, J. F.; Randolph, T. W. High Pressure Fosters Protein Refolding from Aggregates at High Concentrations. *Proc. Natl. Acad. Sci.* **1999**, *96*, 13029−13033.

(22) Kim, Y.-S.; Randolph, T. W.; Seefeldt, M. B.; Carpenter, J. F. High-Pressure Studies on Protein Aggregates and Amyloid Fibrils. *Methods Enzymol.* **2006**, *413*, 237−253.

(23) Sarupria, S.; Ghosh, T.; Garca, A. E.; Garde, S. Studying Pressure Denaturation of a Protein by Molecular Dynamics Simulations. *Proteins: Struct., Funct., Bioinf.* **2010**, *78*, 1641−1651.

(24) Roche, J.; Caro, J. A.; Norberto, D. R.; Barthe, P.; Roumestand, C.; Schlessman, J. L.; Garcia, A. E.; Garca-Moreno, B. E.; Royer, C. A. Cavities Determine the Pressure Unfolding of Proteins. *Proc. Natl. Acad. Sci. U. S. A.* **2012**, *109*, 6945−6950.

(25) Cheung, J. K.; Shah, P.; Truskett, T. M. Heteropolymer Collapse Theory for Protein Folding in the Pressure-Temperature Plane. *Biophys. J.* **2006**, *91*, 2427−2435.

(26) Paschek, D.; Garcia, A. E. Reversible Temperature and Pressure Denaturation of a Protein Fragment: A Replica Exchange Molecular Dynamics Simulation Study. *Phys. Rev. Lett.* **2004**, *93*, 238105−238105-4.

(27) Paschek, D.; Gnanakaran, S.; Garcia, A. E. Simulations of the Pressure and Temperature Unfolding of an Alpha-Helical Peptide. *Proc. Natl. Acad. Sci. U. S. A.* **2005**, *102*, 6765−6770.

(28) Garcia, A. E.; Herce, H.; Paschek, D. In *Annual Reports in Computational Chemistry*; Spellmeyer, D. C., Ed.; Elsevier: Amsterdam, 2006; Vol. 2, pp 83−95.

(29) Paschek, D.; Nymeyer, H.; Garcia, A. E. Replica Exchange Simulation of Reversible Folding/Unfolding of the Trp-Cage Miniprotein in Explicit Solvent: On the Structure and Possible Role of Internal Water. *J. Struct. Biol.* **2007**, *157*, 524−533.

(30) Paschek, D.; Hempel, S.; Garcia, A. E. Computing the Stability Diagram of the Trp-Cage Miniprotein. *Proc. Natl. Acad. Sci.* **2008**, *105*, 17754−17759.

(31) Day, R.; Paschek, D.; Garcia, A. E. Microsecond Simulations of the Folding/Unfolding Thermodynamics of the Trp-Cage Miniprotein. *Proteins: Struct., Funct., Bioinf.* **2010**, *78*, 1889−1899.

(32) Best, R. B.; Hummer, G. Optimized Molecular Dynamics Force Fields Applied to the Helix-Coil Transition of Polypeptides. *J. Phys. Chem. B* **2009**, *113*, 9004−9015.

(33) Neidigh, J. W.; Fesinmeyer, R. M.; Andersen, N. H. Designing a 20-Residue Protein. *Nat. Struct. Mol. Biol.* **2002**, *9*, 425−430.

(34) Gronenborn, A. M.; Filpula, D. R.; Essig, N. Z.; Achari, A.; Whitlow, M.; Wingfield, P. T.; Clore, G. M. A Novel, Highly Stable Fold of the Immunoglobulin Binding Domain of Streptococcal Protein G. *Science* **1991**, *253*, 657−661.

(35) Takekiyo, T.; Shimizu, A.; Kato, M.; Taniguchi, Y. Pressure-Tuning Ft-Ir Spectroscopic Study on the Helix-Coil Transition of Ala-Rich Oligopeptide in Aqueous Solution. *Biochim. Biophys. Acta* **2005**, *1750*, 1−4.

(36) Mori, Y.; Okumura, H. Pressure-Induced Helical Structure of a Peptide Studied by Simulated Tempering Molecular Dynamics Simulations. *J. Phys. Chem. Lett.* **2013**, *4*, 2079−2083.
(37) Salomon-Ferrer, R.; Case, D. A.; Walker, R. C. An Overview of the Amber Biomolecular Simulation Package. *Wiley Interdiscip. Rev.: Comput. Mol. Sci.* **2013**, *3*, 198−210.
(38) Duan, Y.; Wu, C.; Chowdhury, S.; Lee, M. C.; Xiong, G.; Zhang, W.; Yang, R.; Cieplak, P.; Luo, R.; Lee, T.; Caldwell, J.; Wang, J.; Kollman, P. A Point-Charge Force Field for Molecular Mechanics Simulations of Proteins Based on Condensed-Phase Quantum Mechanical Calculations. *J. Comput. Chem.* **2003**, *24*, 1999−2012.
(39) Jorgensen, W. L.; Chandrasekhar, J.; Madura, J. D.; Impey, R. W.; Klein, M. L. Comparison of Simple Potential Functions for Simulating Liquid Water. *J. Chem. Phys.* **1983**, *79*, 926−935.
(40) Hess, B.; Kutzner, C.; van der Spoel, D.; Lindahl, E. GROMACS 4: Algorithms for Highly Efficient, Load-Balanced, and Scalable Molecular Simulation. *J. Chem. Theory Comput.* **2008**, *4*, 435−447.
(41) Best, R. B.; Mittal, J. Balance Between Alpha and Beta Structures in ab initio Protein Folding. *J. Phys. Chem. B* **2010**, *114*, 8790−8798.
(42) Allen, M. P.; Tildesley, D. J. *Computer Simulation of Liquids*; Oxford University Press: New York, 1989.
(43) Berendsen, H. J. C.; Postma, J. P. M.; van Gunsteren, W. F.; DiNola, A.; Haak, J. R. Molecular Dynamics with Coupling to an External Bath. *J. Chem. Phys.* **1984**, *81*, 3684−3690.
(44) Miyamoto, S.; Kollman, P. A. Settle: An Analytical Version of the Shake and Rattle Algorithm for Rigid Water Models. *J. Comput. Chem.* **1992**, *13*, 952−962.
(45) Essmann, U.; Perera, L.; Berkowitz, M. L.; Darden, T.; Lee, H.; Pedersen, L. G. A Smooth Particle Mesh Ewald Method. *J. Chem. Phys.* **1995**, *103*, 8577−8593.
(46) Hess, B. P-LINCS: A Parallel Linear Constraint Solver for Molecular Simulation. *J. Chem. Theory Comput.* **2008**, *4*, 116−122.
(47) Swendsen, R. H.; Wang, J.-S. Replica Monte Carlo Simulation of Spin-Glasses. *Phys. Rev. Lett.* **1986**, *57*, 2607−2609.
(48) Hukushima, K.; Nemoto, K. Exchange Monte Carlo Method and Application to Spin Glass Simulations. *J. Phys. Soc. Jpn.* **1996**, *65*, 1604−1608.
(49) Sugita, Y.; Okamoto, Y. Replica-Exchange Molecular Dynamics Method for Protein Folding. *Chem. Phys. Lett.* **1999**, *314*, 141−151.
(50) Van Gunsteren, W. F.; Berendsen, H. J. C. A Leap-frog Algorithm for Stochastic Dynamics. *Mol. Simul.* **1988**, *1*, 173−185.
(51) Cooke, B.; Schmidler, S. C. Preserving the Boltzmann Ensemble in Replica-Exchange Molecular Dynamics. *J. Chem. Phys.* **2008**, *129*, 164112−164112−17.
(52) Parrinello, M.; Rahman, A. Polymorphic Transitions in Single Crystals: A New Molecular Dynamics Method. *J. Appl. Phys.* **1981**, *52*, 7182−7190.
(53) Frishman, D.; Argos, P. Knowledge-Based Protein Secondary Structure Assignment. *Proteins: Struct., Funct., Genet.* **1995**, *23*, 566−579.
(54) Humphrey, W.; Dalke, A.; Schulten, K. VMD: Visual Molecular Dynamics. *J. Mol. Graphics* **1996**, *14*, 33−38.
(55) Frenkel, D.; Smit, B. *Understanding Molecular Simulation: From Algorithms to Applications*; Academic Press: New York, 2002.
(56) Flyvbjerg, H.; Petersen, H. G. Error Estimates on Averages of Correlated Data. *J. Chem. Phys.* **1989**, *91*, 461−466.
(57) Streicher, W. W.; Makhatadze, G. I. Unfolding Thermodynamics of Trp-Cage, a 20 Residue Miniprotein, Studied by Differential Scanning Calorimetry and Circular Dichroism Spectroscopy. *Biochemistry* **2007**, *46*, 2876−2880.
(58) Muoz, V.; Thompson, P. A.; Hofrichter, J.; Eaton, W. A. Folding Dynamics and Mechanism of Beta-Hairpin Formation. *Nature* **1997**, *390*, 196−199.
(59) Piana, S.; Lindorff-Larsen, K.; Shaw, D. E. Atomic-Level Description of Ubiquitin Folding. *Proc. Natl. Acad. Sci.* **2013**, *110*, 5915−5920.
(60) Ashbaugh, H. S.; Collett, N. J.; Hatch, H. W.; Staton, J. A. Assessing the Thermodynamic Signatures of Hydrophobic Hydration for Several Common Water Models. *J. Chem. Phys.* **2010**, *132*, 124504−124504-7.
(61) Paschek, D.; Day, R.; Garcia, A. E. Influence of Water-Protein Hydrogen Bonding on the Stability of Trp-Cage Miniprotein. a Comparison Between the TIP3P and TIP4P-EW Water Models. *Phys. Chem. Chem. Phys.* **2011**, *13*, 19840−19847.
(62) Nerenberg, P. S.; Head-Gordon, T. Optimizing Protein-Solvent Force Fields to Reproduce Intrinsic Conformational Preferences of Model Peptides. *J. Chem. Theory Comput.* **2011**, *7*, 1220−1230.
(63) Best, R. B.; Mittal, J. Protein Simulations with an Optimized Water Model: Cooperative Helix Formation and Temperature-Induced Unfolded State Collapse. *J. Phys. Chem. B* **2010**, *114*, 14916−14923.
(64) Wang, S.; Tate, M. W.; Gruner, S. M. Protein Crowding Impedes Pressure-Induced Unfolding of Staphylococcal Nuclease. *Biochim. Biophys. Acta* **2012**, *1820*, 957−961.